Mechanical modulation of spin-polarized transport in chiral molecular junctions

Y. Wang,[1,*] W. B. Du,[1,*] X. Liu,[2] J. F. Ren,[1] S. J. Xie,[2] C. Timm,[3,4] C. K. Wang,[1,†] and G. C. Hu[1,‡]

[1]*School of Physics and Electronics, Shandong Normal University, Jinan 250358, China*

[2]*School of Physics, State Key Laboratory of Crystal Materials, Shandong University, Jinan 250100, China*

[3]*Institute of Theoretical Physics, Technische Universität Dresden, 01062 Dresden, Germany*

[4]*Würzburg-Dresden Cluster of Excellence ctd.qmat, Technische Universität Dresden, 01062 Dresden, Germany*

(Received 5 December 2025; revised 4 February 2026; accepted 20 February 2026; published 9 March 2026)

In the framework of tight-binding models and the Green's function method, the mechanical modulation of the chirality-induced spin selectivity (CISS) in chiral molecular junctions is investigated. The results demonstrate that the CISS is weakened monotonically by stretching the molecule, while the change is nonmonotonic in the case of compression. A moderate compression enhances the CISS effect, while a strong compression induces destructive quantum interference (DQI) in the transmission, which generates large spin polarization around the DQI features associated with discrete and irregular spin polarization peaks. We explain the DQI mechanism in terms of interference of multiple paths in a simplified model for the chiral molecule. The variations of long-range electron hopping and spin-orbit coupling under molecular deformation are found to be crucial. For very strong compression, the DQI and the CISS are suppressed. This work proposes a feasible way to modulate the CISS in chiral molecular junctions by deepening our understanding of CISS in the presence of deformation.

DOI: 10.1103/l56v-mspq

I. INTRODUCTION

Organic spintronics is an emerging research field in spintronics that focuses on electronic spin injection and transport in organic materials [1–6]. Chiral molecules are particularly attractive due to their special transport property, namely chirality-induced spin selectivity (CISS) [7–16], where the unpolarized electrons transmitted through the molecule are spin-polarized due to the chiral structure. This effect generates spin polarization (SP) in organics without magnetic ions and in the absence of a magnetic field, which is promising for the future design of organic spintronic devices.

CISS has been widely verified in experiments [15–19], where the magnitude of SP differs in various chiral materials. For example, the SP is only 15% in the early report about bacteriorhodopsin (bR) [19], while a large SP over 60% has been reported in several experiments about double-stranded DNA (dsDNA) [15] and Perylene diimide [20]. A large CISS was also found in some chiral organic-inorganic hybrids [21–23], and even in inorganic chiral CuO and chiral disilicides [24,25]. The preferred orientation of the electron spin depends on the chirality and can be manipulated by illumination [26]. The mechanism of CISS has been investigated in many theoretical works, where different origins have been proposed, including intrinsic chiral geometry [27,28] and the interplay between the spin-orbit coupling (SOC) of electrodes and molecular chirality [29]. In spite of the debate concerning the origin of CISS, several spintronic phenomena based on chiral molecules have been demonstrated, e.g., spin filtering [27,28,30,31], magnetoresistance [26,32–34], rectification [20], quantum interference [35], and spin-light-emitting diodes [2,36].

The modulation and especially the enhancement of the SP generated by chiral molecules is an interesting issue since strong CISS benefits further application of chiral molecules. Experimental reports have shown that the SP of the current is affected by the substrate [19,30], molecular length [16,28,37], and illumination [26]. Theoretical studies have found that the SP is related to the strength of SOC, dephasing, and electron hopping [27,28], which are all related to the species of chiral molecules and to their structural deformation. In molecular electronics, mechanical manipulation is a frequently used method to modulate molecular structure and electronic transport, which can be implemented with atomic force microscopes. Force-induced modulation of molecular conductance or quantum interference in molecular junctions has been reported [38–40]. The mechanical response of chiral molecules was also addressed in several experiments. For example, it was reported that the elastic modulus of an oligopeptide molecular layer is about 12 GPa [41]. Using a magnetic tip, an increase of the tunneling current and a decrease of the SP were observed upon compressing the chiral junction [42]. In spite of this experimental progress, the force-induced changes of chiral structure and its effect on the CISS have not been addressed theoretically in any detail, except for a few simple discussions of the effects of structure deformation on the SOC strength and transmission [27,43].

In this paper, we construct a tight-binding model for a molecular junction composed of a single-helical chiral molecule sandwiched between two nonmagnetic electrodes. The effect of a force F on the junction is investigated,

*These authors contributed equally to this work.

†Contact author: ckwang@sdnu.edu.cn

‡Contact author: hgc@sdnu.edu.cn

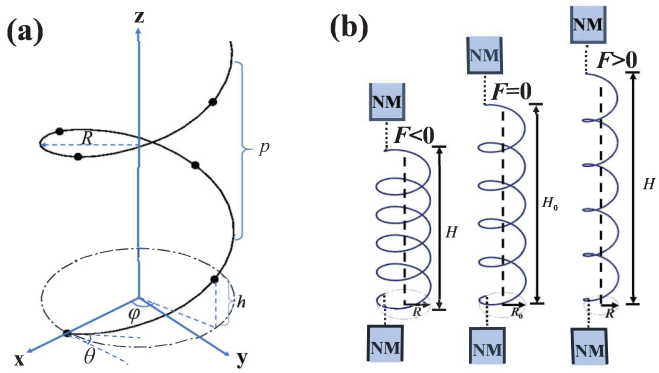

FIG. 1. (a) Geometric structure of the chiral molecule. (b) Schematic illustration of the deformation and of the radius R and height H of a chiral molecule under a force.

including both tension ($F > 0$) and compression ($F < 0$). The force-induced changes of the total molecular energy and chiral structure are investigated. Then the spin-polarized transmission through the chiral molecular junction is calculated and the dependence of the SP on the force is studied. The paper is organized as follows: In Sec. II, the model Hamiltonian and the theoretical method are introduced. In Sec. III, the results are presented and discussed. A brief conclusion is given in Sec. IV.

II. MODEL AND METHODS

We consider a single-helical molecule sandwiched between two nonmagnetic metallic electrodes. The structure of the molecule is illustrated in Fig. 1(a). The molecule is described by the tight-binding Hamiltonian [27,28]

$$H_{\mathrm{m}} = \sum_{n=1}^{N-1}\sum_{j=1}^{N-n} t_j (c_n^{\dagger} c_{n+j} + \mathrm{H.c.}) + \sum_{n}^{N-1}\sum_{j=1}^{N-n} 2is_j \cos(\varphi_{n,j}^{-})(c_n^{\dagger}\sigma_{nj} c_{n+j} + \mathrm{H.c.}). \quad (1)$$

The first term is the electron hopping term, where t_j represents the electronic hopping integral between sites n and $n+j$. t_j is assumed to decay exponentially with the distance l_j between two sites with decay length l_c, which can be expressed as $t_j = t_1 e^{-(l_j - l_1)/l_c}$. t_1 is the hopping integral for nearest neighbors. l_j is calculated by $l_j = \sqrt{[2R\sin(j\varphi/2)]^2 + (jh)^2}$. R is the radius of the helical structure. ϕ and h are the twist angle and displacement along the z direction for two neighboring sites. h can be obtained from the total height of the molecule H and the number of sites N as $h = H/(N-1)$. $c_n^{\dagger} = (c_{n\uparrow}^{\dagger}, c_{n\downarrow}^{\dagger})$ and $c_n = \binom{c_{n\uparrow}}{c_{n\downarrow}}$ are the creation and annihilation operators for the electrons at site n, respectively. The second term denotes SOC. s_j is the renormalized SOC strength with $s_j = s_1 e^{-(l_j - l_1)/l_c}$, which also decays with the distance between sites similarly to t_j. $\varphi_{n,j}^{\pm} = (\varphi_{n+j} \pm \varphi_n)/2$ are relative angles, where $\varphi_n = (n-1)\varphi$ is the cylindrical coordinate of site n. $\sigma_{nj} = (\xi\sigma_x \sin\varphi_{n,j}^{+} - \sigma_y \cos\varphi_{n,j}^{+})\sin\theta_j + \xi\sigma_z\cos\theta_j$, where σ_x, σ_y, and σ_z are Pauli matrices. $\theta_j = \arccos[2R\sin(j\varphi/2)/l_j]$ is the helix angle as shown in Fig. 1(a). $\xi = 1(-1)$ represents the right-handed (left-handed) chirality of the molecule.

The chiral molecule is connected to two nonmagnetic electrodes via terminal sites. Without force, the chiral molecule stays in the initial state with length H_0, radius R_0, pitch p_0, helix angle θ_0, and twist angle φ_0. A force applied along the z axis will stretch or compress the molecule according to the direction of the force: Under a force F, the change of molecular height is $\Delta H = H - H_0$, as shown in Fig. 1(b). The longitudinal strain is $\varepsilon = (H - H_0)/H_0$. During the deformation process, we assume that the arc length l_a between two neighboring sites is unchanged, whereas the radius and pitch are modulated [44,45]. For example, as shown in Fig. 1(b), when the molecular junction is stretched, the radius shrinks with increasing height, whereas the radius increases and the height decreases in the case of compression. The radius is calculated as $R = R_0(1-\nu\varepsilon)$, where ν is the Poisson ratio of the helix and is usually taken as 0.5 [45,46]. With the values of H and R, the helix angle θ and the twist angle φ can be obtained through the geometric relations $l_a \sin\theta = H/(N-1)$ and $l_a\cos\theta = R\varphi$. The nearest-neighbor hopping integral t_1 is also assumed to be unchanged because we notice that the change of the distance l_1 between the nearest-neighbor sites is negligible ($<1.5\%$).

The relation between the force and the molecular deformation can be obtained from the total molecular energy. The total molecular energy includes both the electronic energy and the lattice elastic energy with $E_{\mathrm{t}} = E_{\mathrm{e}} + E_{\mathrm{lat}}$. The electronic energy E_{e} can be obtained by summing up the energy of all occupied eigenlevels. Here half-filling is considered. The eigenlevels are calculated from the electronic Schrödinger equation, which is solved in Wannier representation with the Hamiltonian in Eq. (1). All other contributions to the energy, including the energies of electrons in lower-lying bands and the Coulomb repulsion between the nuclei, are subsumed in the elastic energy E_{lat}. We make a harmonic approximation for this energy, thereby assuming that any anharmonicity stems from the partially filled band. Note that this is not essential for the results of this paper, which will be expressed in terms of the change of molecular height, not of the applied force. The elastic energy is taken to consist of two parts [47–49],

$$E_{\mathrm{lat}} = \int_0^L \left[\frac{B}{2}(\kappa - \kappa_0)^2 + \frac{C}{2}(\tau - \tau_0)^2\right] ds, \quad (2)$$

where κ and τ describe the curvature and the torsion of the molecule, respectively. The two quantities can be calculated via

$$\kappa = \frac{R}{R^2 + \left(\frac{p}{2\pi}\right)^2}, \quad (3)$$

$$\tau = \frac{\frac{p}{2\pi}}{R^2 + \left(\frac{p}{2\pi}\right)^2}. \quad (4)$$

B and C are the bending and twisting stiffnesses, respectively, where the values are taken as 250 and 480 pN nm^2 according to previous work [50]. L is the contour length. The integration is performed along the arc length coordinate s. The relation between the external force and the total molecular energy E_{t} is expressed as [50,51] $F = \frac{\partial E_{\mathrm{t}}}{\partial H}$.

Given a change ΔH of the molecular height, the structural deformation and all the structural parameters can be determined. Then the electronic structure is calculated by the Schrödinger equation, and the total molecular energy as well as the corresponding force F can be obtained.

Next, the spin-polarized transport property will be investigated. Using the Green's function method, the electron transmission coefficient from lead p with spin s' to lead q with spin s can be calculated as [52,53] $T_{qs,ps'} = \mathrm{Tr}[\Gamma_{qs} G^r \Gamma_{ps'} G^a]$. Here, $G^r = [G^a]^\dagger = [E - H_m - \sum_{qs(q=L,R,V)} \Sigma^r_{qs}]^{-1}$ is the single-particle Green's function, E is the incident electron energy, $\Gamma_{qs} = i[\Sigma^r_{qs} - \Sigma^a_{qs}]$ is the broadening function, and $\Sigma^{r(a)}_{qs}$ is the retarded (advanced) self-energy due to the coupling to lead q. Note that here virtual electrodes attached to every site are introduced to simulate the dissipation due to the environment, which is necessary to generate the SP [34,54–56]. In the wide-band limit, the broadening function is assumed to be energy-independent by setting $\Sigma^r_{L/Rs} = -i\Gamma_{L/R}/2$ for the left and right leads and $\Sigma^r_{Vs} = -i\Gamma_d/2$ for the virtual leads, respectively. Physically, the broadening in the Green's functions results from coherent tunneling of electrons into and back out of the leads.

In addition, the incoherent, sequential combinations of transmissions between various (virtual) leads is often described by an effective transmission coefficient [31,54,57]. The spin-resolved effective transmission coefficient between the left and right leads is given by [31]

$$T_{\mathrm{eff},s}(\varepsilon) = \sum_{s'} T_{Rs,Ls'} + \sum_{\mu,\nu} \left[\left(\sum_{s'} T_{Rs,\mu s'} \right) W^{-1}_{\mu,\nu} \left(\sum_{s,s'} T_{\nu s,Ls'} \right) \right], \quad (5)$$

where $W^{-1}_{\mu,\nu}$ can be obtained by inverting the matrix $W_{\mu,\nu} = \sum_{\gamma(\neq\mu)} (\sum_{s,s'} T_{\gamma s,\mu s'}) \delta_{\mu\nu} - (\sum_{s,s'} T_{\mu s,\nu s'})(1 - \delta_{\mu\nu})$. In Eq. (5), the first term is the coherent tunneling, whereas the second term is the incoherent contribution which reflects the electronic dephasing by the virtual leads. Note that in Refs. [54,57], a spinless model is considered. However, in Ref. [31] and in our model, the spin is included and it is assumed that the tunneling of electrons into the virtual leads completely scrambles their spin. The SP of transmission is then given by $P_s = (T_{\mathrm{eff}\uparrow} - T_{\mathrm{eff}\downarrow})/(T_{\mathrm{eff}\uparrow} + T_{\mathrm{eff}\downarrow})$.

The parameters used for the numerical calculations are chosen as follows: For the chiral molecule, $N = 30$, $t_1 = 1.0$ eV, $s_1 = 0.12t_1$, and $l_c = 0.09$ nm, which are typical values used for chiral molecules [27]. The initial geometric parameters are taken from α-helix protein molecules as $R_0 = 0.23$ nm, $H_0 = 4.35$ nm, $p_0 = 0.54$ nm, and $\varphi_0 = \frac{5\pi}{9}$, which have been widely used in previous works [27,43]. For the real and virtual electrodes in the case of the wide-band limit [58], the broadening parameters are set to $\Gamma_{L/R} = 1.0t_1$ and $\Gamma_d = 0.006t_1$, respectively.

III. RESULTS AND DISCUSSION

We start from the equilibrium state of the chiral molecular junction without force. The spin-resolved transmission as well as its SP is plotted in Fig. 2 as functions of energy. A continuous transmission spectrum with peaks is observed, where the maximum transmission coefficient reaches 0.9. Spin splitting of transmission occurs especially for the peaks near the Fermi energy, which indicates the appearance of CISS. The transmission spectrum is spin-up polarized below −0.19 eV and spin-down polarized above this energy. The maximum SP reaches about 0.09 and −0.17 in the two regions, respectively. The magnitude of SP is comparable to other calculations [27,59,60] and experimental reports [19,61].

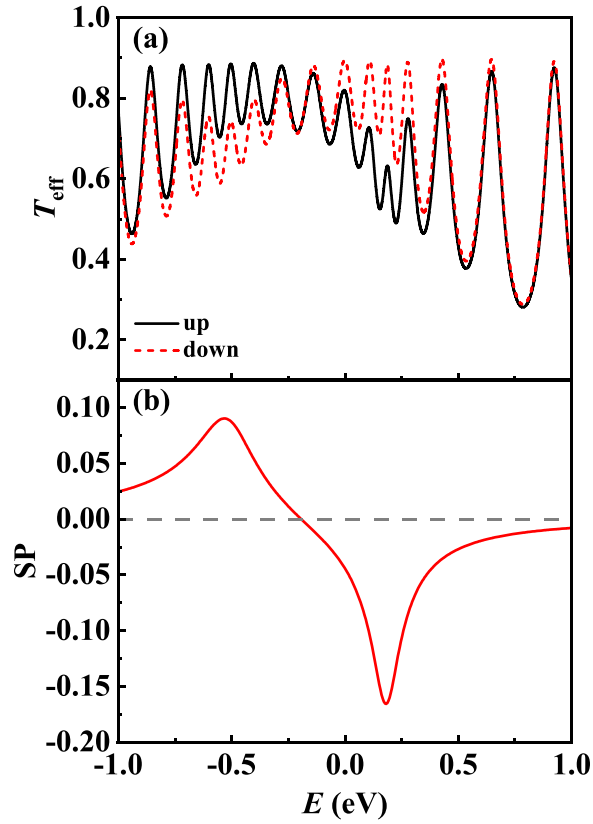

FIG. 2. (a) Spin-resolved transmission of the device without force. (b) Energy-dependent SP of transmission.

By applying a force, the molecular height as well as the structure are modified. According to an experimental report [62], a chiral molecule can be fully strecthed to a one-dimensional structure, but there is no related report concerning the maximum compression of a chiral molecule. Upon strong compression, the chiral molecule might buckle. This buckling might be prevented by using a molecular monolayer instead of an isolated molecule. Here, we take the deformation of the molecular height to be within ±10 Å.

To establish a relation between the molecular deformation and the force, we first show the change of molecular energy and the corresponding force F for various molecular heights. As shown in Fig. 3(a), the deformation of the molecule, under either stretching or compression, leads to an increase of the total molecular energy, which is dominated by the lattice energy. The electronic energy decreases upon stretching but shows a nonmonotonic dependence under compression, exhibiting a slight increase for a small compression of about 3 Å and then

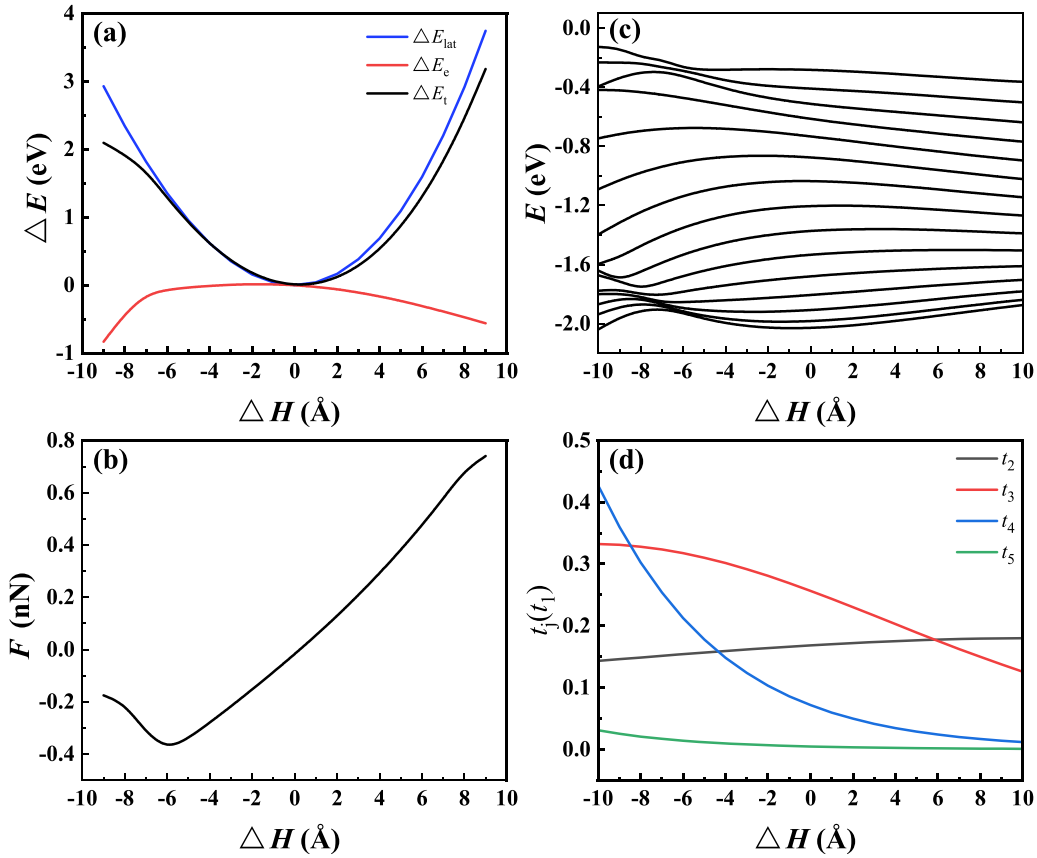

FIG. 3. (a) Evolution of electronic energy E_e, lattice energy E_{lat}, and total molecular energy E_t with the change ΔH of molecular height. Here, ΔE is the energy difference between the deformed molecule and the initial one defined as $\Delta E = E(\Delta H) - E(0)$. (b) Corresponding force for each height. (c) Eigenvalues of occupied states. (d) Long-range electronic hopping integrals in units of the nearest-neighbor hopping t_1.

starting to decrease. In particular, we observe a quick drop beyond 6 Å. Figure 3(b) shows the corresponding external force, which increases almost linearly with the deformation, except for a minimum at −6 Å. The magnitude of the force is on the order of nN, which is close to the value reported in experiments [62] and first-principles calculations for molecular junctions [51].

Since the change of electronic states induced by deformation is crucial for the spin-polarized transport, we explore it in more detail below. In Figs. 3(c) and 3(d), we plot the changes of eigenvalues of occupied states and the dominant long-range electronic hopping integrals as a function of molecular height. We find that the band becomes narrower for increasing height in the range of [−2, 10] Å, while an obvious qualitative change occurs during the compression process, especially around −6 Å, corresponding to the drop of electronic energy. This change is due to the evolution of electronic hopping integrals under deformation. As depicted in Fig. 3(d), deformation has little influence on t_2 and t_5, while pronounced changes are found for t_3 and t_4, especially an exponential decay of t_4 with height. Thus, as the molecule is stretched from the equilibrium state, the band structure is dominated by the nearest hopping t_1 as for a one-dimensional chain, while the longer-range hopping is weakened because of the decay of t_3 and t_4, leading to a reduction of the bandwidth. However, upon strong compression, the significant increase of t_3 and t_4 enhances the hybridization between loops of the helix, which drives the structure away from the one-dimensional one and causes qualitative changes of the electronic structure. It should be mentioned that the above evolution of electronic structure with structural deformation is based on the single-orbital model, where the hopping integral decays exponentially with distance. If a multiorbital model is considered for each atom, which will be more realistic for specific molecules, the dependence of the hopping integral on the separation of atoms will also be sensitive to orbital character, especially under compression. For example, the reduced helix pitch will selectively enhance the hopping between orbitals oriented along the molecular axis. This will further influence the electronic sates near the Fermi energy. Such treatment is complicated and beyond the present scope.

Now we discuss the spin-polarized transport through the chiral molecule in the presence of stretching and compression. In Figs. 4(a)–4(f), the spin-resolved transmission is first investigated in the case of moderate deformation ($|\Delta H| < 5$ Å). When the molecule is stretched, the transmission spectrum remains similar to the equilibrium state, except for a slight shift of peaks caused by the slight energy shift of frontier orbitals. Moreover, the spin splitting of the transmission around the Fermi energy is reduced. This is reasonable since the

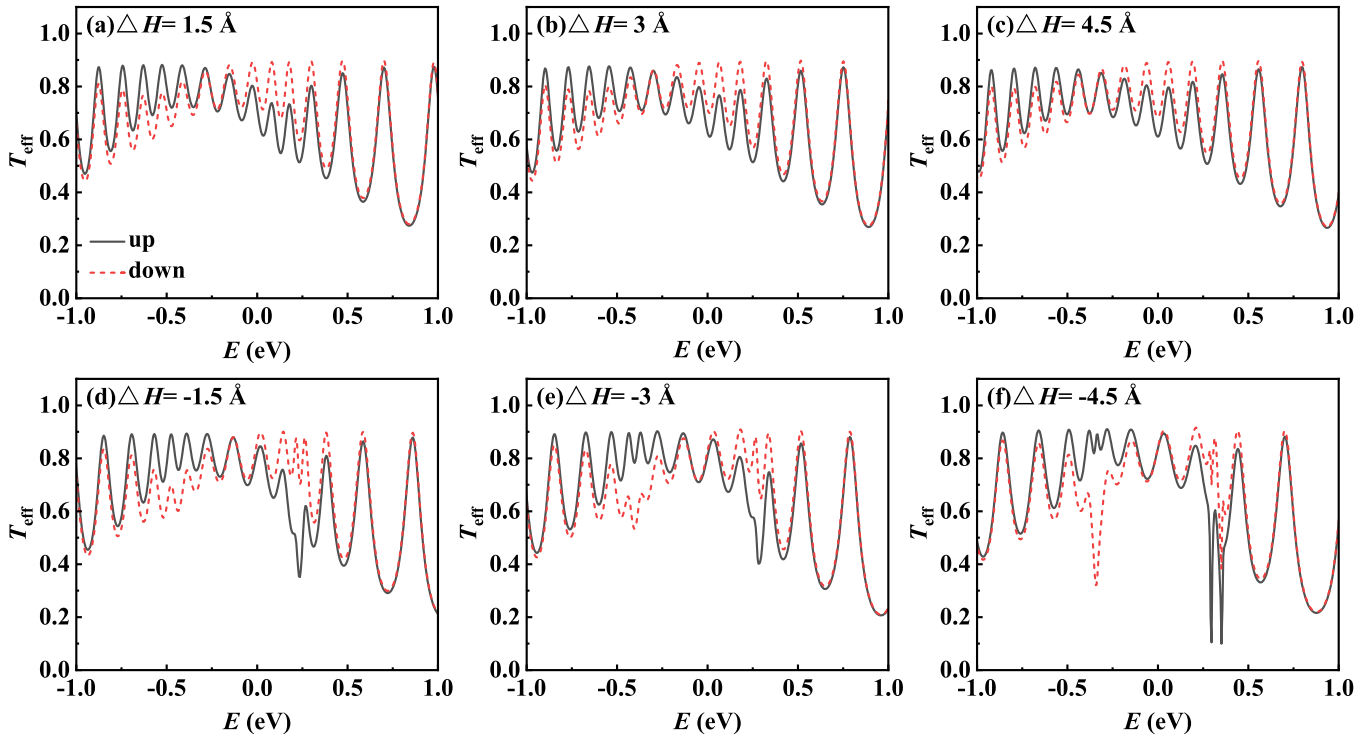

FIG. 4. Spin-resolved transmission in the presence of moderate stretching and compression. Panels (a)–(c) pertain to stretching, and (d)–(f) pertain to compression.

long-range hopping as well as the chirality are weakened by the stretching. In the limit of extreme stretching, the molecule tends towards a one-dimensional chain, and the chirality as well as the CISS vanishes.

In the case of compression, the transmission becomes irregular due to the nonlinear evolution of the electronic structure. Although the SP of the transmission around the Fermi energy is reduced, several transmission dips begin to emerge for different spins, e.g., around 0.25 and −0.3 eV, which leads to an obvious enhancement of the SP around these energies. These dips arise from the quantum interference of multipath transport, as discussed in detail later.

In Fig. 5, we plot the SP of transmission near the Fermi energy for moderate deformation. As shown in Fig. 5(a), in the presence of stretching, both the positive and negative SP peaks around the Fermi energy move towards lower energy accompanied by a reduction of their magnitude. An opposite evolution is observed in the case of compression, where a blueshift occurs for the SP peaks and their magnitude is significantly enhanced. In Fig. 5(b), we plot the change of the maximum magnitude of the positive and negative SP peaks with deformation. When the molecule becomes shorter, a monotonic increase is observed for the positive peak, which is especially rapid below −3.0 Å. For the negative peak, the SP decreases from 0.2 to 0.05 upon the stretching, while it increases to over 0.8 at −2.5 Å. Thus, a compression of about 6% of the total molecular height may lead to an enhancement of the SP to four times its value without compression, which realizes a rapid mechanical modulation of the SP. Beyond that, oscillations of the SP occur for further compression. The results indicate that the CISS of the chiral molecule can be significantly enhanced by moderate compression.

The change of the SP for moderate deformation can be understood as follows. The CISS in chiral molecules is mainly controlled by the SOC and the long-range hopping. In the presence of moderate deformation, the long-range hopping terms decay for stretching and increase for compression, as demonstrated in Fig. 3(d). Due to the similar exponential dependence on the distance for the SOC, an analogous evolution can be expected for the SOC strength in the presence of deformation. An increase of SP with the SOC strength has been demonstrated in previous work [27]. Thus, the increase (decrease) of the two interactions induced by compression (stretching) is responsible for the enhancement (reduction) of the CISS.

Now let us discuss the CISS in the situation of strong compression, where the molecular electronic structure is modified dramatically, as shown in Fig. 3(c). Figure 6 gives the spin-resolved transmission at several deformations starting from $\Delta H = -6$ Å. It is found that as the compression grows from −6 to −10 Å, the discrete transmission peaks become more and more irregular. Simultaneously, additional spin-resolved transmission dips appear, the positions and depths of which vary with the deformation. We note that the SP for most transmission peaks becomes insignificant, whereas large SP occurs at energies with transmission dips.

Transmission dips are known as prominent characteristics of destructive quantum interference (DQI) between different electronic transport paths in molecular devices, which has been widely observed in aromatic and heterocyclic molecular

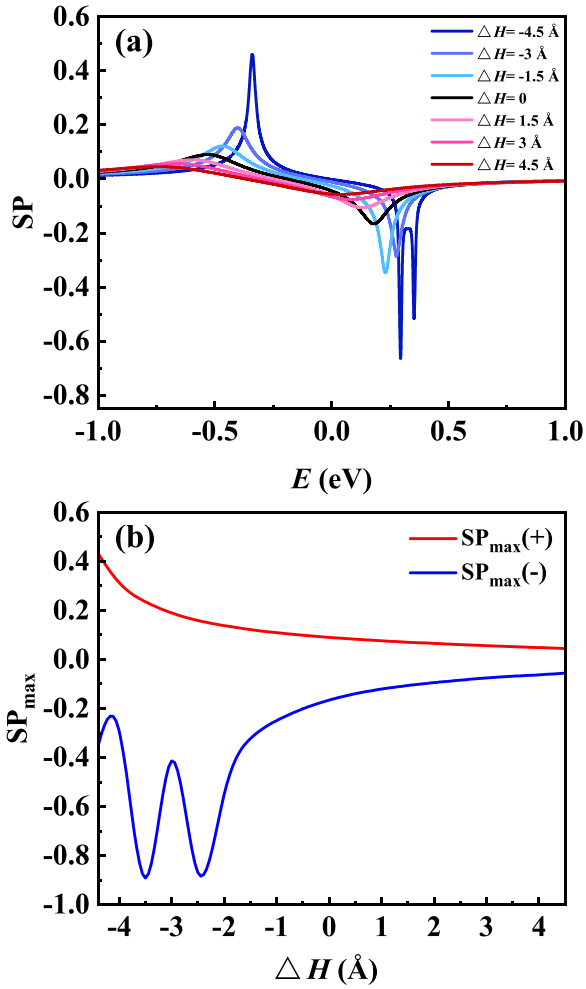

FIG. 5. (a) SP of transmission near the Fermi energy for moderate deformation. (b) Maxima of SP from panel (a) as functions of deformation.

devices [63–66]. In the present work, DQI in the chiral molecule emerges from the enhancement of multipath transport effects under strong compression. More specifically, it is induced by the increased long-rang hopping as shown in Fig. 3(d), especially for t_3 and t_4. For example, for a compression of -10 Å, t_3 and t_4 reach 0.33 and 0.43 eV, respectively, and thus reach nearly half of the nearest-neighbor hopping t_1 so that the direct transport between loops is strongly enhanced.

To clearly show the details of quantum interference in the case of strong compression, we present in Fig. 7(a), a schematic diagram for the interference between interloop hopping and helix transport caused by t_4 because t_4 is the largest hopping integral at the strong compression of -10 Å. In the present model, the chiral molecule contains roughly four sites per loop. The two paths contributing to the interference can be labeled as the interloop hopping P($i \to i+4$) and the helix transport P($i \to i+1 \to i+2 \to i+3 \to i+4$), as shown in Fig. 7(a). To simplify the analysis, we neglect the SOC since the DQI from multipath transport should be robust even without SOC. As shown in Fig. 7(b), the DQI dips still exist

TABLE I. Quantum interference occurring between different loops at an energy of 0 with transmission dip and -0.5 eV without dip, as shown in Fig. 7(b). The former is mainly contributed by the HOMO and LUMO and the latter by the HOMO-4 and HOMO-5. For other paths starting from $i = 2$, 3, and 4, the numbers of DQI at $E = 0$ are 5/7, 3/6, 3/6, while at $E = -0.5$ eV the corresponding numbers of DQI are 2/7, 1/6, 1/6, respectively. The details are not shown.

	HOMO	LUMO	0 eV	HOMO-4	HOMO-5	-0.5 eV
$C_1C_5^*$	<0	<0	DQI	>0	<0	CQI
$C_5C_9^*$	<0	<0	DQI	<0	>0	CQI
$C_9C_{13}^*$	>0	<0	CQI	>0	<0	CQI
$C_{13}C_{17}^*$	<0	<0	DQI	<0	>0	CQI
$C_{17}C_{21}^*$	<0	>0	CQI	>0	<0	CQI
$C_{21}C_{25}^*$	<0	<0	DQI	<0	<0	DQI
$C_{25}C_{29}^*$	<0	<0	DQI	>0	>0	DQI

around the Fermi energy, in spite of the modified transmission and spin degeneracy due to the absence of SOC.

We focus on the dip at the Fermi energy of $E = 0$ shown in Fig. 7(b). According to previous works on DQI [63–66], the DQI near the Fermi energy can be understood from the Green's function contributed by the highest occupied molecular orbital (HOMO) and the lowest unoccupied molecular orbital (LUMO), which is approximately given by $G_{IJ}(E) \approx \frac{C_{I,\mathrm{HOMO}}C_{J,\mathrm{HOMO}}^*}{E-\varepsilon_{\mathrm{HOMO}}} + \frac{C_{I,\mathrm{LUMO}}C_{J,\mathrm{LUMO}}^*}{E-\varepsilon_{\mathrm{LUMO}}}$. Here, $C_{I(J),\mathrm{HOMO}}$ and $C_{I(J),\mathrm{LUMO}}$ are the coefficients of the HOMO and LUMO at the two terminal sites for the two interfering paths, which can be obtained from their wave functions displayed in Figs. 7(c) and 7(d). $\varepsilon_{\mathrm{HOMO}}$ ($\varepsilon_{\mathrm{LUMO}}$) is the eigenenergy of the HOMO (LUMO). If the two terms in the Green's function have opposite signs for a specific energy, DQI will occur. Otherwise, constructive quantum interference (CQI) pertains. For the energy between the LUMO and HOMO, where the signs of the energy denominators are opposite for the two terms, DQI is examined for each loop by checking the signs of coefficients of the HOMO and LUMO. Specifically, we take the paths starting from $i = 1$ as an example and give the results in Table I. DQI appears for five out of seven loops. DQI for other paths starting from $i = 2$,3,4 is also examined, where the DQI occurs for more than half of all loops. As a comparison, we also check the quantum interference at $E = -0.5$ eV without transmission dip, which is located between the HOMO-4 and HOMO-5 states and dominated by these two states. The result clearly shows CQI for the majority for all loops. Hence, it is plausible that the transmission dip is truly induced by the DQI. Due to the coexistence with CQI for several loops, the DQI dips are not as prominent as reported for other quantum interference junctions with only two paths [63–66], for which the magnitude of transmission may be strongly suppressed by a factor reaching 10^{-8}. Note that when the chiral molecular junction is not compressed, the DQI will not be prominent even if the coefficients of the orbitals meet the criterion for DQI since the interloop hopping and thus the multipath transport are much weaker.

Although the above argument provides evidence for DQI, it should be mentioned that DQI in chiral molecules is much

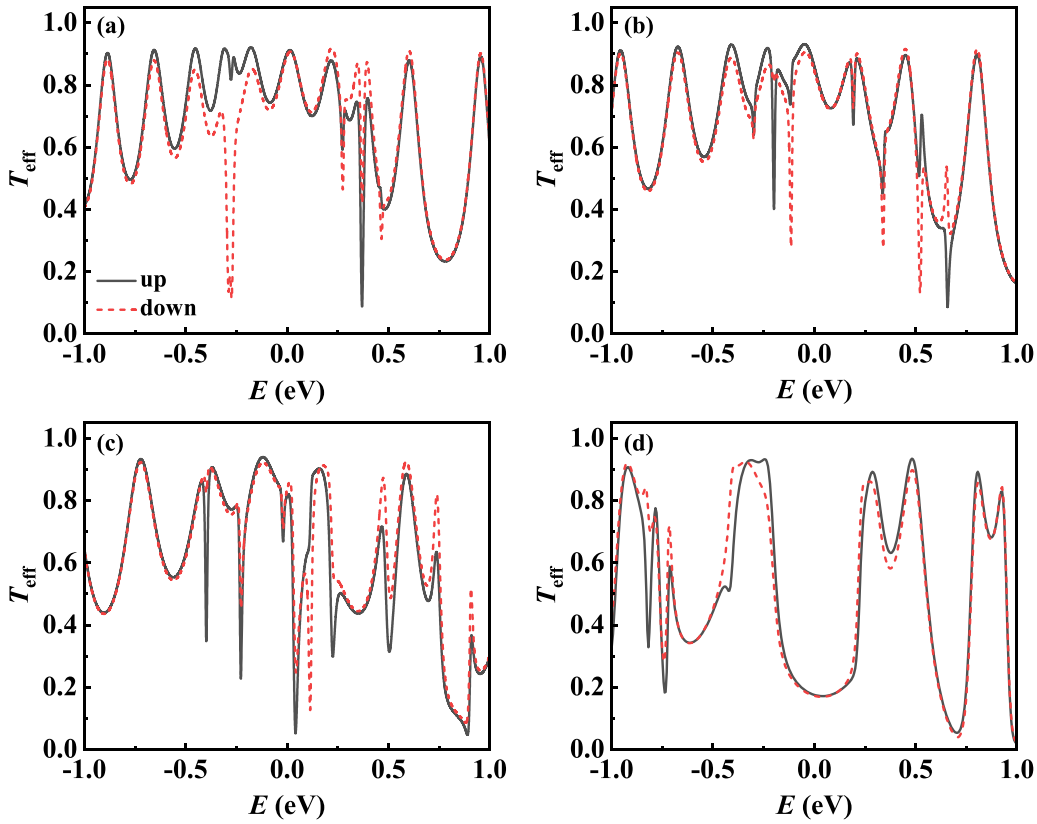

FIG. 6. Spin-resolved transmission for strong compression. Panels (a)–(d) correspond to $\Delta H = -6, -8, -10$, and -15 Å, respectively.

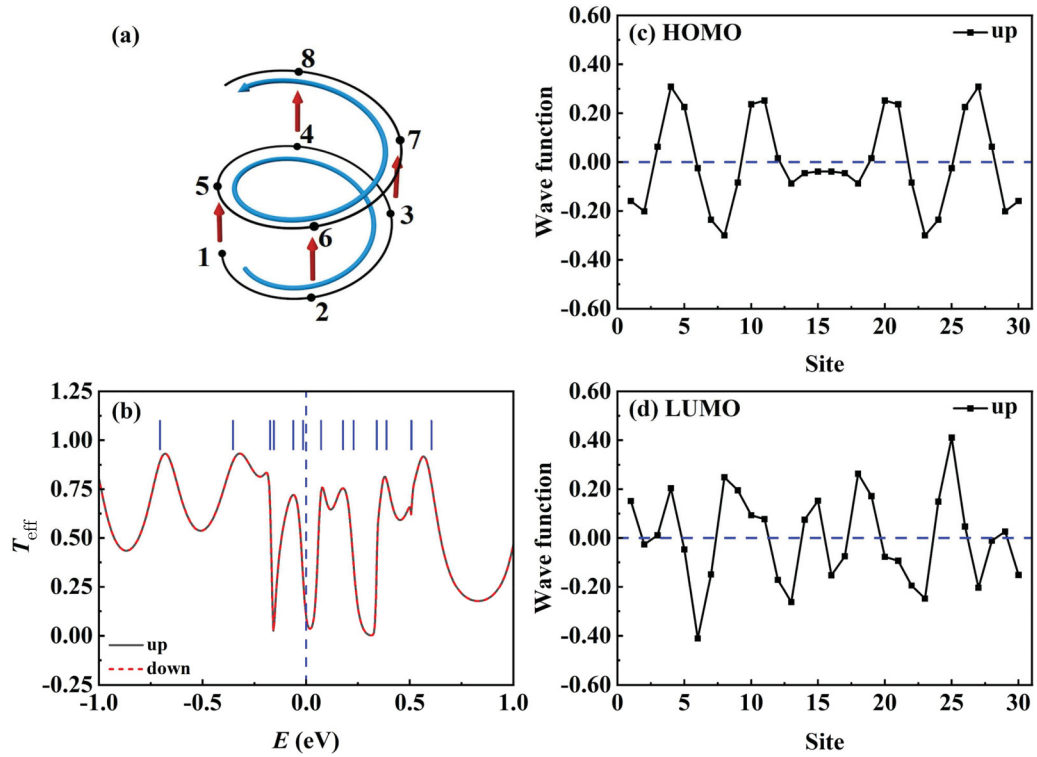

FIG. 7. (a) Schematic diagram of quantum interference between interloop hopping and helix transport induced by t_4. The two interfering paths are P(1 → 5) and P(1 → 2 → 3 → 4 → 5), P(2 → 6) and P(2 → 3 → 4 → 5 → 6), etc. (b) Transmission near the Fermi energy for strong compression with $\Delta H = -10$ Å. The SOC is set to zero. The short lines indicate the molecular eigenvalues. Panels (c) and (d) show the wave functions for the HOMO and LUMO states, respectively.

more complicated if we further include the paths contributed by t_2, t_3, and t_5. Moreover, since each long-rang hopping shows a different dependence on the deformation, the multi-path transport keeps changing during the compression, which makes the DQI features depend on the deformation. Recently, DQI in circular chiral molecules induced by different contact sites of two leads has been studied theoretically [35]. The magnitude of transmission dips in our work is comparable with theirs.

Thus, compression-induced DQI provides an additional way to enhance CISS in chiral molecular junctions. Due to the energy dependence of this enhancement, control of the on-site energy at the molecular sites would be desirable for the experimental verification. Such control is, in principle, possible by using a gate electrode. Additionally, we emphasize that the large SP is an integrated effect from the spin splitting generated by the chiral molecule and the sharp DQI dips. A similar effect has been reported for magnetic molecular junctions [63], where the spin splitting is contributed by hybridized interfacial states, while the DQI dip is generated by the heterocyclic molecules.

A subsequent physical issue is whether strong DQI features continue to exist when the chiral molecule is further compressed. To check this, we give the result for -15 Å. Although the structural stability of the chiral molecule at this large deformation is uncertain, the result is helpful to understand the evolution of the CISS in the limit of strong compression. As shown in Fig. 6(d), we find that the number of the dips decreases compared with Fig. 6(c). The spin splitting of the transmission spectrum near the Fermi energy is strongly reduced, which makes the CISS nearly invisible. The reason is that in this case, the hybridization between the loops becomes very strong. For example, now t_3 and t_4 are 0.32 and 0.95 eV, respectively. The strength of t_4 is comparable to the nearest-neighbor hopping along the chain. In this case, the direct electron transport between the loops becomes more important than the transport along the helix. In this regime, the chiral molecule acts more like several coupled one-dimensional chains along the z direction so that there is no reason for strong effects based on chirality.

The energy-dependent SP of the molecule in the case of strong compression is shown in Fig. 8(a). Obviously, compared to Fig. 5(a), the SP develops more discrete peaks and becomes more irregular with the increase of deformation. Narrow SP peaks arise around the Fermi energy, contributed by the spin-resolved DQI dips, as mentioned above. As the deformation changes from -6 to -10 Å, the SP peaks approach the Fermi energy, and a large SP over 0.8 close to the Fermi energy is achieved at $\Delta H = -10$ Å. At $\Delta H = -15$ Å, the two SP peaks closest to the Fermi energy are much reduced to less than 0.15. Figure 8(b) shows the evolution of the SP over the whole range of compressions. The initial two SP peaks are enhanced and shifted to higher energies with the increase of deformation. At around -5 Å, the negative SP peak begins to split into separate peaks, which indicates the emergence of narrow peaks with large SP. According to Figs. 4(d) and 5(a), we know that they are caused by DQI. The splitting of the positive SP peak appears at around -7 Å. Beyond this compression, the discrete SP peaks survive in a larger energy

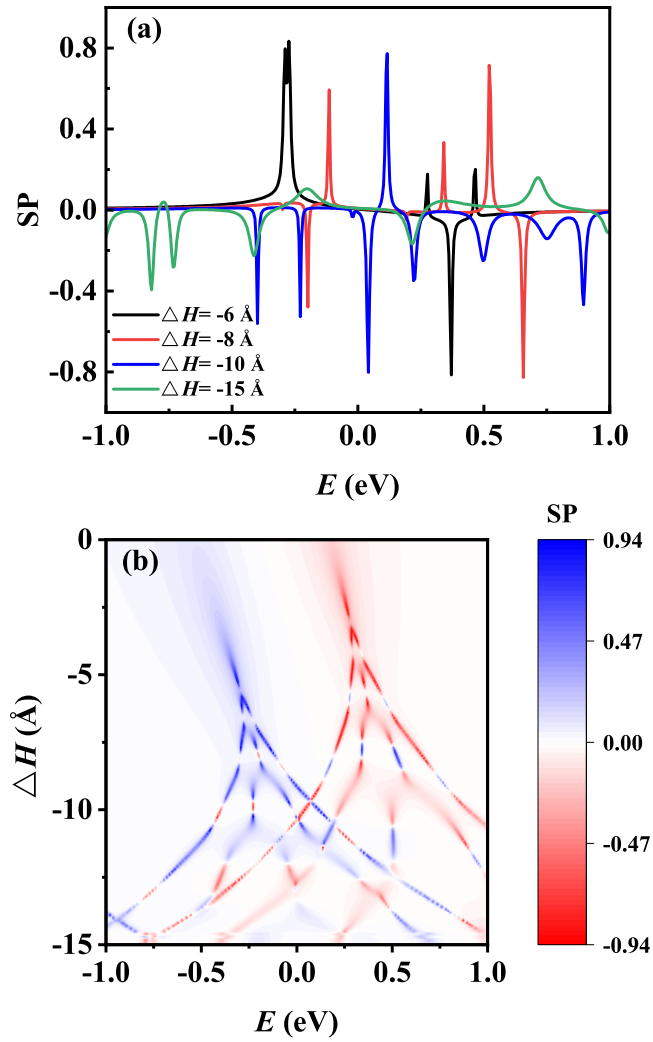

FIG. 8. (a) SP of transmission near the Fermi energy for strong compression with $\Delta H = -6, -8, -10$, and -15 Å. (b) Evolution of SP for different energies and deformations for compression.

range. If the deformation is over -12 Å, no significant SP peaks are found close to the Fermi energy. Hence, we find that a large SP adjacent to the Fermi energy is expected for deformations in the range from -9 to -11 Å.

Since the compression-induced DQI arises from the interference, the influence of the dephasing term in our model should be considered. In Fig. 9, we show the spin-resolved transmission at $\Delta H = -10$ Å for different dephasing strengths. As Γ_d increases to $0.02t_1$, the DQI dips are still observed but their number and depth are reduced compared to Fig. 6(c). When Γ_d continues to increase, the DQI features are further weakened and eventually become invisible at $\Gamma_d = 0.05t_1$, which means that the loss of electronic phase coherence impedes the formation of DQI.

Finally, it should be mentioned that a previous measurement of oligopeptide molecular junctions reported a compression-induced decay of CISS [42]. However, in that work a magnetic tip was adopted. Although such a structure is beneficial for measuring SP in terms of conductance, the observed SP is indeed a magnetoresistance effect. The

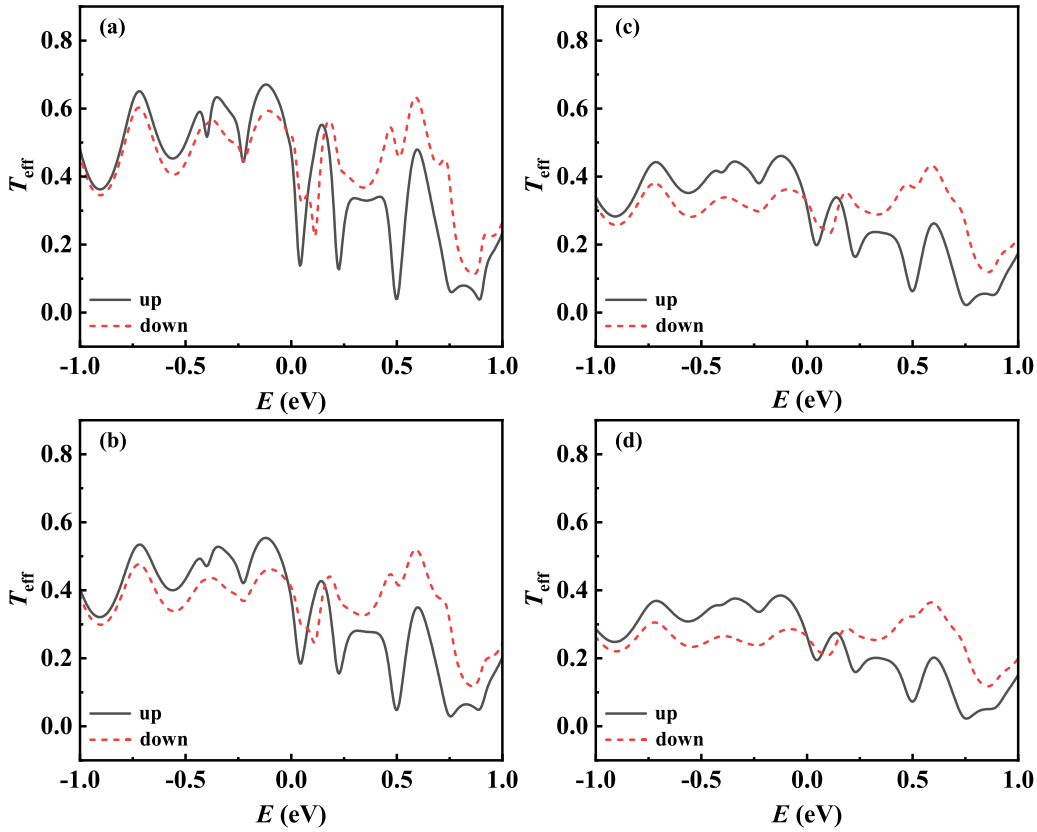

FIG. 9. Spin-resolved transmission at $\Delta H = -10$ Å for a dephasing strength of (a) $\Gamma_d = 0.02t_1$, (b) $\Gamma_d = 0.03t_1$, (c) $\Gamma_d = 0.04t_1$, and (d) $\Gamma_d = 0.05t_1$, respectively.

effect of spin alignment between the chiral molecule and the ferromagnetic electrode may cover the real change of SP arising from the chiral molecule and thus may be different from our calculated results with nonmagnetic electrodes. Furthermore, in our work, the discussed compression effect is limited to the deformation of the chiral molecule along the z axis, which is expected to be feasible with the utilization of atomic force or scanning tunneling microscopes [42,62,67]. In experiments, compression-induced buckling of the molecule is also possible. Additionally, a molecular monolayer could be used to suppress the buckling, as noted in Sec. III, but in this case uniform tilting of the molecules as well as interactions between molecules could weaken their deformation. Such complex situations are beyond the present simulation. Finally, the chirality transfer or chiral proximity effect between chiral materials and nonmagnetic electrodes is an important issue for the CISS according to previous works [68–70]. The stretching or compression of the junction will modify not only the intrinsic chirality of the molecule but also the molecule-electrode coupling strength, which in principle can be used to modulate chiral proximity effects. Such effects are not considered here but deserve to be investigated in future studies.

IV. SUMMARY AND CONCLUSIONS

In summary, the mechanical modulation of CISS in chiral molecular junctions by an applied force is investigated based on a tight-binding model and the Green's function method. The effect of the force on the molecular structure is described by structural deformation in the form of stretching or compression. In the presence of a force, the total molecular energy increases due to the contribution of the lattice elastic energy, while the electronic states show distinct response for stretching or compression. In the case of stretching, the electronic energy band becomes narrower and the total electronic energy is lowered, whereas compression induces a nonmonotonic change of the band structure and the electronic energy. These changes are explained by the evolution of electronic long-range hopping upon deformation of the molecule induced by the force.

The corresponding transmission calculation reveals that in the presence of stretching, the CISS is weakened, accompanied by a redshift in energy. These effects are attributed to the decay of electronic long-range hopping and SOC, which are crucial for the SP. In the case of compression, a nonmonotonic change of the CISS is obtained. For moderate compression, the SP peaks near the Fermi energy increase, accompanied by a blueshift in energy, due to the increase of long-range hopping and SOC. For strong compression, DQI features emerge in the transmission spectra caused by the enhancement of multipath transport. As a result, an enhanced CISS around the DQI features emerges. The compression-induced DQI is analyzed and verified using a model for multipath interference between frontier orbitals. The DQI is modified and suppressed by dephasing. In the limit of strong compression, the DQI features vanish and the CISS becomes very weak since in this regime the direct electron transport between the loops is strong and the chiral characteristic is suppressed.

This work describes a feasible way to modulate the CISS in chiral molecular junctions and deepens our understanding of the mechanism of CISS in the presence of molecular deformations.

ACKNOWLEDGMENTS

Support from the National Natural Science Foundation of China (Grants No. 12474212 and No. 12274264), the Shandong Provincial Natural Science Foundation (Grant No. ZR2025MS09), and the scholarship fund of China Scholar Council are gratefully acknowledged. C.T. gratefully acknowledges support by the Deutsche Forschungsgemeinschaft through the Collaborative Research Center Grant No. SFB 1143, project A04, project ID 247310070, and the Würzburg-Dresden Cluster of Excellence ctd.qmat, EXC 2147, project ID 390858490.

DATA AVAILABILITY

The data that support the findings of this article are not publicly available because of legal restrictions preventing unrestricted public distribution. The data are available from the authors upon reasonable request.

[1] S. Sanvito, Molecular spintronics, Chem. Soc. Rev. **40**, 3336 (2011).
[2] I. Zutic, J. Fabian, and S. D. Sarma, Spintronics: Fundamentals and applications, Rev. Mod. Phys. **76**, 323 (2004).
[3] J. Sinova and I. Zutic, New moves of the spintronics tango, Nat. Mater. **11**, 368 (2012).
[4] D. Li and G. Yu, Innovation of materials, devices, and functionalized interfaces in organic spintronics, Adv. Funct. Mater. **31**, 2100550 (2021).
[5] H. Q. Zhang, D. Li, Y. Y. Miao, S. Qiu, G. P. Zhang, J. F. Ren, C. K. Wang, and G. C. Hu, Molecular rectification assisted by spin-polarized hybrid interfacial states, Phys. Lett. A **443**, 128200 (2022).
[6] X. N. Sun, A. Bedoya-Pinto, Z. P. Mao, M. Gobbi, W. J. Yan, Y. L. Guo, A. Atxabal, R. Llopis, G. Yu, Y. Q. Liu, A. Chuvilin, F. Casanova, and L. E. Hueso, Active morphology control for concomitant long distance spin transport and photoresponse in a single organic device, Adv. Mater. **28**, 2609 (2016).
[7] B. P. Bloom, Y. Paltiel, R. Naaman, and D. H. Waldeck, Chiral induced spin selectivity, Chem. Rev. **124**, 1950 (2024).
[8] Z. X. Shang, T. H. Liu, Q. Q. Yang, S. N. Cui, K. L. Xu, Y. Zhang, J. X. Deng, T. R. Zhai, and X. L. Wang, Chiral-molecule-based spintronic devices, Small **18**, 2203015 (2022).
[9] F. Evers, A. Aharony, N. Bar-Gill, O. Entin-Wohlman, P. Hedegård, O. Hod, P. Jelinek, G. Kamieniarz, M. Lemeshko, K. Michaeli, M. Vladimiro, R. Naaman, Y. Paltiel, S. Refaely-Abramson, O. Tal, J. Thijssen, M. Thoss, J. M. van Ruitenbeek, L. Venkataraman, D. H. Waldeck, B. H. Yan, and L. Kronik, Theory of chirality induced spin selectivity: Progress and challenges, Adv. Mater. **34**, 2106629 (2022).
[10] S. H. Yang, R. Naaman, Y. Paltiel, and S. S. P. Parkin, Chiral spintronics, Nat. Rev. Phys. **3**, 328 (2021).
[11] R. Naaman, Y. Paltiel, and D. H. Waldeck, Chiral molecules and the electron spin, Nat. Rev. Chem. **3**, 250 (2019).
[12] K. Ray, S. P. Ananthavel, D. H. Waldeck, and R. Naaman, Asymmetric scattering of polarized electrons by organized organic films of chiral molecules, Science **283**, 814 (1999).
[13] I. Carmeli, V. Skakalova, R. Naaman, and Z. Vager, Magnetization of chiral monolayers of polypeptide: A possible source of magnetism in some biological membranes, Angew. Chem. Int. Ed. **41**, 761 (2002).
[14] S. G. Ray, S. S. Daube, G. Leitus, Z. Vager, and R. Naaman, Chirality-induced spin-selective properties of self-assembled monolayers of DNA on gold, Phys. Rev. Lett. **96**, 036101 (2006).
[15] B. Göhler, V. Hamelbeck, T. Z. Markus, M. Kettner, G. F. Hanne, Z. Vager, R. Naaman, and H. Zacharias, Spin selectivity in electron transmission through self-assembled monolayers of double-stranded DNA, Science **331**, 894 (2011).
[16] Z. T. Xie, T. Z. Markus, S. R. Cohen, Z. Vager, R. Gutierrez, and R. Naaman, Spin specific electron conduction through DNA oligomers, Nano Lett. **11**, 4652 (2011).
[17] D. M. Sterner, J. M. Abendroth, K. M. Cheung, M. Ye, M. S. El Hadri, E. E. Fullerton, and P. S. Weiss, Differential charging in photoemission from mercurated DNA monolayers on ferromagnetic films, Nano Lett. **20**, 1218 (2020).
[18] S. Mishra, A. K. Mondal, S. Pal, T. K. Das, E. Z. B. Smolinsky, G. Siligardi, and R. Naaman, Length-dependent electron spin polarization in oligopeptides and DNA, J. Phys. Chem. C **124**, 10776 (2020).
[19] D. Mishra, T. Z. Markus, R. Naaman, M. Kettner, B. Göhler, H. Zacharias, N. Friedman, M. Sheves, and C. Fontanesi, Spin-dependent electron transmission through bacteriorhodopsin embedded in purple membrane, Proc. Natl. Acad. Sci. USA **110**, 14872 (2013).
[20] C. H. Ko, Q. Zhu, G. Bullard, F. Tassinari, M. Morisue, R. Naaman, and M. J. Therien, Electron spin polarization and rectification driven by chiral perylene diimide-based nanodonuts, J. Phys. Chem. Lett. **14**, 10271 (2023).
[21] Z. Bian, K. Kato, T. Ogoshi, Z. Cui, B. Sa, Y. Tsutsui, S. Seki, and M. Suda, Hybrid chiral MoS_2 layers for spin-polarized charge transport and spin-dependent electrocatalytic applications, Adv. Sci. **9**, 2201063 (2022).
[22] U. Huizi-Rayo, J. Gutierrez, J. M. Seco, V. Mujica, I. Diez-Perez, J. M. Ugalde, A. Tercjak, J. Cepeda, and E. San Sebastian, An ideal spin filter: Long-range, high-spin selectivity in chiral helicoidal 3-dimensional metal organic frameworks, Nano Lett. **20**, 8476 (2020).
[23] H. Lu, C. Xiao, R. Song, T. Li, A. E. Maughan, A. Levin, R. Brunecky, J. J. Berry, D. B. Mitzi, V. Blum, and M. C. Beard, Highly distorted chiral two-dimensional tin iodide perovskites for spin polarized charge transport, J. Am. Chem. Soc. **142**, 13030 (2020).
[24] K. B. Ghosh, W. Zhang, F. Tassinari, Y. Mastai, O. Lidor-Shalev, R. Naaman, P. Möllers, D. Nürenberg, H. Zacharias, J. Wei, E. Wierzbinski, and D. H. Waldeck, Controlling chemical

selectivity in electrocatalysis with chiral CuO-coated electrodes, J. Phys. Chem. C **123**, 3024 (2019).

[25] H. Shishido, R. Sakai, Y. Hosaka, and Y. Togawa, Detection of chirality-induced spin polarization over millimeters in polycrystalline bulk samples of chiral disilicides $NbSi_2$ and $TaSi_2$, Appl. Phys. Lett. **119**, 182403 (2021).

[26] M. Suda, Y. Thathong, V. Promarak, H. Kojima, M. Nakamura, T. Shiraogawa, M. Ehara, and H. M. Yamamoto, Light-driven molecular switch for reconfigurable spin filters, Nat. Commun. **10**, 2455 (2019).

[27] A. M. Guo and Q. F. Sun, Spin-dependent electron transport in protein-like single-helical molecules, Proc. Natl. Acad. Sci. USA **111**, 11658 (2014).

[28] A. M. Guo and Q. F. Sun, Spin-selective transport of electrons in DNA double helix, Phys. Rev. Lett. **108**, 218102 (2012).

[29] S. Alwan and Y. Dubi, Spinterface origin for the chirality-induced spin-selectivity effect, J. Am. Chem. Soc. **143**, 14235 (2021).

[30] R. Naaman, Y. Paltiel, and D. H. Waldeck, Chiral molecules and the spin selectivity effect, J. Phys. Chem. Lett. **11**, 3660 (2020).

[31] X. Liu, X. H. Liu, and S. J. Xie, Chiral resistance effect in an organic helical heterojunction device, Appl. Phys. Lett. **121**, 113502 (2022).

[32] K. Kondou, M. Shiga, S. Sakamoto, H. Inuzuka, A. Nihonyanagi, F. Araoka, M. Kobayashi, S. Miwa, D. Miyajima, and Y. C. Otani, Chirality-induced magnetoresistance due to thermally driven spin polarization, J. Am. Chem. Soc. **144**, 7302 (2022).

[33] K. Kondou, S. Miwa, and D. Miyajima, Spontaneous spin selectivity in chiral molecules at the interface, J. Magn. Magn. Mater. **585**, 171157 (2023).

[34] X. Yang, C. H. van der Wal, and B. J. van Wees, Detecting chirality in two-terminal electronic nanodevices, Nano Lett. **20**, 6148 (2020).

[35] S. Chen and H. H. Fu, Spin-dependent destructive and constructive quantum interference associated with chirality-induced spin selectivity in single circular helix molecules, J. Phys. Chem. Lett. **14**, 11076 (2023).

[36] M. P. Hautzinger, X. Pan, S. C. Hayden, J. Y. Ye, Q. Jiang, M. J. Wilson, A. J. Phillips, Y. Dong, E. K. Raulerson, I. A. Leahy, C.-S. Jiang, J. L. Blackburn, J. M. Luther, Y. Lu, K. Jungjohann, Z. V. Vardeny, J. J. Berry, K. Alberi, and M. C. Beard, Room-temperature spin injection across a chiral perovskite/III–V interface, Nature (London) **631**, 307 (2024).

[37] L. L. Zhang, Y. Y. Hao, W. Qin, S. J. Xie, and F. Y. Qu, Chiral-induced spin selectivity: A polaron transport model, Phys. Rev. B **102**, 214303 (2020).

[38] V. S. Aradhya, J. S. Meisner, M. Krikorian, S. Ahn, R. Parameswaran, M. L. Steigerwald, C. Nuckolls, and L. Venkataraman, Dissecting contact mechanics from quantum interference in single-molecule junctions of stilbene derivatives, Nano Lett. **12**, 1643 (2012).

[39] X. H. Li, Y. Zheng, Y. Zhou, Z. Y. Zhu, J. Y. Wu, W. H. Ge, Y. X. Zhang, Y. Q. Ye, L. C. Chen, J. Shi, J. Y. Liu, J. Bai, Z. T. Liu, and W. J. Hong, Supramolecular transistors with quantum interference effect, J. Am. Chem. Soc. **145**, 21679 (2023).

[40] C. Nef, P. Frederix, J. Brunner, C. Schönenberger, and M. Calame, Force-conductance correlation in individual molecular junctions, Nanotechnology **23**, 365201 (2012).

[41] J. Pawlowski, J. Juhaniewicz, D. Tymecka, and S. Sek, Electron transfer across α-helical peptide monolayers: Importance of interchain coupling, Langmuir **28**, 17287 (2012).

[42] V. Kiran, S. R. Cohen, and R. Naaman, Structure dependent spin selectivity in electron transport through oligopeptides, J. Chem. Phys. **146**, 092302 (2017).

[43] H. N. Wu, X. Wang, Y. J. Zhang, G. Y. Yi, and W. J. Gong, Enhancement of spin polarization in transport through protein-like single-helical molecules, Appl. Phys. A **122**, 626 (2016).

[44] S. V. Salazar, V. Mujica, and E. Medina, Spin-orbit coupling modulation in DNA by mechanical deformations, Chimia **72**, 411 (2018).

[45] J. D. Torres, R. Hidalgo-Sacoto, S. Varela, and E. Medina, Mechanically modulated spin-orbit couplings in oligopeptides, Phys. Rev. B **102**, 035426 (2020).

[46] T. R. Pan, A. M. Guo, and Q. F. Sun, Spin-polarized electron transport through helicene molecular junctions, Phys. Rev. B **94**, 235448 (2016).

[47] D. A. Kessler and Y. Rabin, Stretching instability of helical springs, Phys. Rev. Lett. **90**, 024301 (2003).

[48] C. W. Wolgemuth and S. X. Sun, Elasticity of α-helical coiled coils, Phys. Rev. Lett. **97**, 248101 (2006).

[49] J. T. Pham, J. Lawrence, G. M. Grason, T. Emrick, and A. J. Crosby, Stretching of assembled nanoparticle helical springs, Phys. Chem. Chem. Phys. **16**, 10261 (2014).

[50] J. Gore, Z. Bryant, M. Nöllmann, M. U. Le, N. R. Cozzarelli, and C. Bustamante, DNA overwinds when stretched, Nature (London) **442**, 836 (2006).

[51] F. Sun, R. Liu, Y. Q. Suo, L. L. Niu, H. Y. Fu, W. F. Ji, and Z. L. Li, First principle study on stretching and breaking process of single-molecule junction: Terminal group effect, Acta Phys. Sin. **68**, 178502 (2019).

[52] S. Datta, *Electronic Transport in Mesoscopic Systems* (Cambridge University Press, Cambridge, 1995).

[53] D. Ferry and S. M. Goodnick, *Transport in Nanostructures* (Cambridge University Press, Cambridge, 1997).

[54] X. Q. Li and Y. J. Yan, Electrical transport through individual DNA molecules, Appl. Phys. Lett. **79**, 2190 (2001).

[55] J. H. Wei and K. S. Chan, Charge transport in polyguanine-polycytosine DNA molecules, J. Phys.: Condens. Matter **19**, 286101 (2007).

[56] M. Kilgour and D. Segal, Charge transport in molecular junctions: From tunneling to hopping with the probe technique, J. Chem. Phys. **143**, 024111 (2015).

[57] J. L. D'Amato and H. M. Pastawski, Conductance of a disordered linear chain including inelastic scattering events, Phys. Rev. B **41**, 7411 (1990).

[58] A. M. Guo and Q. F. Sun, Sequence-dependent spin-selective tunneling along double-stranded DNA, Phys. Rev. B **86**, 115441 (2012).

[59] Y. Z. Liu, J. W. Xiao, J. Koo, and B. H. Yan, Chirality-driven topological electronic structure of DNA-like materials, Nat. Mater. **20**, 638 (2021).

[60] M. A. Sierra, D. Sánchez, R. Gutierrez, G. Cuniberti, F. Domínguez-Adame, and E. Díaz, Spin-polarized electron transmission in DNA-like systems, Biomolecules **10**, 49 (2020).

[61] M. Kettner, B. Göhler, H. Zacharias, D. Mishra, V. Kiran, R. Naaman, C. Fontanesi, D. H. Waldeck, S. Sek, J. Pawlowski, and J. Juhaniewicz, Spin filtering in electron

transport through chiral oligopeptides, J. Phys. Chem. C **119**, 14542 (2015).

[62] M. A. Lantz, S. P. Jarvis, H. Tokumoto, T. Martynski, T. Kusumi, C. Nakamura, and J. Miyake, Stretching the α-helix:: a direct measure of the hydrogen-bond energy of a single-peptide molecule, Chem. Phys. Lett. **315**, 61 (1999).

[63] S. Qiu, Y. Y. Miao, G. P. Zhang, J. F. Ren, C. K. Wang, and G. C. Hu, Manipulating current spin polarization in magnetic single-molecule junctions via destructive quantum interference, J. Phys. Chem. C **124**, 12144 (2020).

[64] M. Taniguchi, M. Tsutsui, R. Mogi, T. Sugawara, Y. Tsuji, K. Yoshizawa, and T. Kawai, Dependence of single-molecule conductance on molecule junction symmetry, J. Am. Chem. Soc. **133**, 11426 (2011).

[65] K. Yoshizawa, An orbital rule for electron transport in molecules, Acc. Chem. Res. **45**, 1612 (2012).

[66] X. Zhao, V. Geskin, and R. Stadler, Destructive quantum interference in electron transport: A reconciliation of the molecular orbital and the atomic orbital perspective, J. Chem. Phys. **146**, 092308 (2017).

[67] A. C. Aragonès, E. Medina, M. Ferrer-Huerta, N. Gimeno, M. Teixidó, J. L. Palma, N. Tao, J. M. Ugalde, E. Giralt, I. Díez-Pérez, and V. Mujica, Measuring the spin-polarization power of a single chiral molecule, Small **13**, 1602519 (2017).

[68] M. A. Haque, A. Grieder, S. P. Harvey, R. Brunecky, J. Y. Ye, B. Addison, J. Zhang, Y. Dong, Y. Xie, M. P. Hautzinger, H. H. Walpitage, K. Zhu, J. L. Blackburn, Z. V. Vardeny, D. B. Mitzi, J. J. Berry, S. R. Marder, Y. Ping, M. C. Beard, and J. M. Luther, Remote chirality transfer in low-dimensional hybrid metal halide semiconductors, Nat. Chem. **17**, 29 (2024).

[69] Y. Liu, R. Shrestha, K. Denisov, D. Ayala, M. van Schilfgaarde, W. Nie, and I. Žutić, Unconventional spintronics from chiral perovskites, Adv. Funct. Mater. **35**, e09127 (2025).

[70] M. Du, X. Liu, X. Liu, and S. Xie, Chirality transfer induced spin selectivity effect in a molecule-metal heterojunction, Phys. Rev. B **108**, 125419 (2023).